



TUM

TECHNISCHE UNIVERSITÄT MÜNCHEN
INSTITUT FÜR INFORMATIK

Biologically Plausible Spatial Navigation Based on Border Cells

Camillo Heye, Zhenshan Bing, Alois Knoll

TUM-I2294

DEPARTMENT OF INFORMATICS

TECHNISCHE UNIVERSITÄT MÜNCHEN

Bachelor's Thesis in Informatics

**Biologically Plausible Spatial Navigation
Based on Border Cells**

Camillo Heye

DEPARTMENT OF INFORMATICS

TECHNISCHE UNIVERSITÄT MÜNCHEN

Bachelor's Thesis in Informatics

**Biologically Plausible Spatial Navigation
Based on Border Cells**

**Biologisch plausible räumliche Navigation
basierend auf Grenzzellen**

Author: Camillo Heye
Supervisor: Prof.Dr.-Ing.habil. Alois Knoll
Advisor: Dr.rer.nat. Zhenshan Bing
Submission Date: 28.08.2021

I confirm that this bachelor's thesis in informatics is my own work and I have documented all sources and material used.

Munich, 28.08.2021

Camillo Heye

Acknowledgments

Abstract

Biologically plausible spatial navigation (NeuralSLAM) tries to solve spatial navigation tasks by modelling and implementing our brain's spatial navigation system [1]. In 1971 O'Keefe and Dostrovsky discovered the Place Cell, a spatially selective cell that reacts to certain locations in an environment, helping the animal to locate itself [21]. Since then many additional spatially selective cell types have been discovered in rodents. These are neurons whose receptive fields reference some aspect of an organism's location, state of motion, pose or relationship to environmental features (such as boundaries, landmarks and other objects) [6]. The interaction of these neurons create the brain's spatial navigation system. The neuron populations coding for extended boundaries in the environmental surrounding include egocentric boundary cells (eBC), which code for boundaries in peri-personal space (i.e. left, right, ahead), border cells (BC) and boundary vector cells (BVC), the latter two coding in allocentric coordinates (independent from facing direction, world-centered).

None of the models that incorporate boundary coding cells are simulated in environments unknown to the agent. Here a network based on the BB-model by Bicanski and Burgess [5], is provided that encodes egocentric boundary information and transforms it into an allocentric reference frame via a head direction modulated transformation circuit. The network incorporates a biologically plausible head direction network, which decodes current heading direction based on angular velocity in real-time. Together with simulated perception of environmental surroundings, the model is applicable to produce eBC and BVC during simulation in unknown environments. Since there are many models which simulate BVC firing as input to PC firing this model could be extended to a bigger network, in which the output of this model - BVC's neuronal firing profiles - drive PC firing. In addition the sensory inputs (which are yet to be fully understood [6]), could be modelled in a more biologically plausible way.

Contents

Acknowledgments	iii
Abstract	iv
1. Introduction	1
2. Biological Properties of Boundary Coding and Head Direction Cells	3
2.1. Biological Properties of Boundary Coding Cells	3
2.2. Biological properties of Head Direction Cells	6
3. Related Work	7
3.1. BB-Model of spatial memory and imagery	7
4. Methodology	10
4.1. Neuron Models	10
4.1.1. Boundary Coding Neurons	10
4.1.2. Head Direction Cells	11
4.2. HDC Network Architecture	12
4.3. BC Network Architecture	13
4.3.1. Activity Profile	13
4.3.2. Architecture	15
4.3.3. Transformation Circuit (TR)	16
4.4. Synaptic Weights and Training	19
4.4.1. Synaptic Weights	19
4.5. Perception	20
5. Results and Discussion	21
5.1. Simulation Setup	21
5.2. Simulation Results	23
5.3. Rate Differences	31
5.4. Biological Plausibility	35
6. Conclusion and Future Work	36
6.1. Conclusion	36

Contents

6.2. Future Work	36
A. Computational Details	38
List of Figures	40
List of Tables	44
Bibliography	45

1. Introduction

Simultaneous localization and mapping (SLAM), as an artificial approach to solve spatial navigation tasks, has been greatly investigated and implemented in the domain of robotics and autonomous driving, with the rapid developments of sensors, algorithms, and the enhanced computing capability of deep neural networks [1]. But no system solves spatial navigation tasks as good as our brain does, the approach that is trying to model our brain's areas responsible for spatial navigation is called biologically plausible spatial navigation (NeuralSLAM), and differs greatly from artificial SLAM approaches.

In 1971 O'Keefe and Dostrovsky discovered the first neuron population, which is involved in spatial navigation, the place cells (PC). The PC is a spatially selective cell that reacts to certain locations in an environment, helping the animal to locate itself [21]. Since then many additional spatially selective cell types have been discovered in rodents: that is, neurons whose receptive fields reference some aspect of an organism's location, state of motion, pose or relationship to environmental features (such as boundaries, landmarks and other objects)[6]. The cells which have been subject to the most research are:

- Place Cells: neurons that fire when the animal occupies certain locations in an environment [21].
- Grid Cells (GC): neurons that fire whenever the animal's position is alligned with any vertex of a hexagonal grid spanning the surface of the environment [13] (see Figure 3.2).
- Head Direction cells: neurons that are tuned to a specific allocentric heading direction, and show the highest activity when the agent is facing in that particular direction [29].
- Boundary coding cells: neurons which fire when any kind of movement preventing boundary is encountered [18].

The focus of this thesis are boundary coding cells. There are egocentric boundary cells (eBC) [16] [2] which code in an egocentric reference frame and can be found in retrosplenial cortex (RSC), parietal cortex (PCX), striatum (STM), postrhinal cortex (POR) and lateral entorhinal cortex (LEC), border cells (BC) [26] [27] found in medial

entorhinal cortex (MEC) and boundary vector cells (BVCs) [18] which code in an allocentric reference frame and are found in subiculum [6]. Allocentric means world-centered (independent from the animals heading direction (north, east, south, west)). Egocentric boundary cells are coded relative to the facing direction of the agent, i.e. their receptive fields are in their peri-personal space (left, right, ahead) and rotate together with the agents heading direction [6]. Transforming the head-centered (egocentric) perceptual information into an allocentric reference frame is achieved by using the current heading direction which is provided by the head direction cell (HDC). This transformation is predicted to take place in the RSC [5], [9], and recent recordings from RSC further support that prognosis [2].

BVCs are essential for, and have been shown to drive PC firing [14], [12], [3], [4]. Most models only model BVCs as input to drive PC firing, and no model, which incorporates boundary coding cells, is simulated in environments unknown to the agent. Here I provide a network that encodes egocentric boundary information and transforms it into an allocentric reference frame via a head direction modulated transformation circuit, based on the BB-Model by Bicanski and Burgess [5]. The network incorporates a biologically plausible head direction network, which decodes current heading direction based on angular velocity in real-time. The model is tested in a simulation in which a robot navigates through an unknown environment, and evaluated based on the results. Together with simulated perception of the surroundings, the model is applicable to produce real-time eBC and BVC firing during simulation in unknown environments.

2. Biological Properties of Boundary Coding and Head Direction Cells

2.1. Biological Properties of Boundary Coding Cells

Each boundary coding cell responds to any kind of elongated boundary, which is located at a specific distance and direction from the agent with a different firing rate. That area for which a given BC fires is called its receptive field. The further away the receptive field the bigger it gets (see Figure 2.1). The existence of neurons, responsible for boundary detection was first predicted by [14], and later [4] strengthened that prediction. [4] proposed that a neuron, called the Boundary Vector Cell (BVC) is what mainly drives the firing of the previously mentioned place cell. In later work, border cells (BC) [26] [27], boundary vector cells [18] and egocentric boundary cells (eBC) [16] [2] have been discovered in the rat brain, delivering proof that those predictions were right. A boundary can be a wall, a drop-off edge, or any kind of elongated obstacle [18]. Different to the other boundary coding cells, border cells only respond to proximate boundaries (whisking range of rats), and only fire for boundaries which block the path of the animal [17]. The spatial receptive fields of these neurons correspond to vectors, which indicate distance and direction (direction either independent of heading direction (BVC, BC) or relative to heading direction (eBC)) in space, for which the presence of a boundary will drive the neuron to fire (see Figures 2.2, 2.3). So in contrast to place and grid cells which have a receptive field centered on the agents current position (see Figure 2.4, 3.2), boundary coding cells have their receptive fields covering locations around the agent [6]. The boundary vector cell and the border cell express these vectorial codes in allocentric coordinates. The egocentric boundary cells are coded relative to the facing direction of the agent. All the boundary coding cells get their input from sensory perception, i.e. from their whiskers, and the visual system. In addition some cells showed sensitivity to boundaries behind the animal implying that a mnemonic component is also incorporated [6].

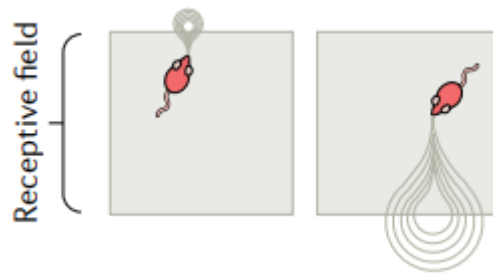


Figure 2.1.: Two receptive fields. The further away the boundary the bigger the receptive field [6].

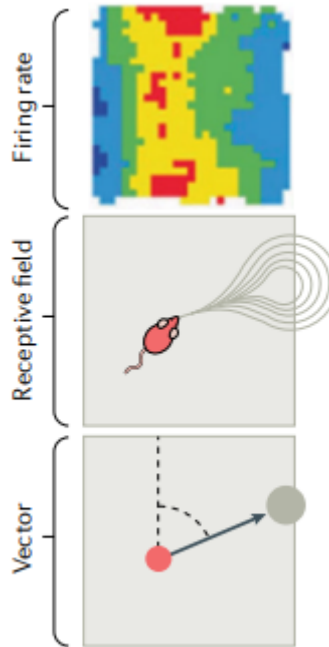


Figure 2.2.: (Top) Firing rate map of a boundary vector cell. (Middle) Illustration of the receptive field of this cell, which is located at a fixed distance and direction from the agent. (Bottom) Vector pointing from the agent's location to the receptive field. When the receptive field is occupied by a boundary, the neuron fires. [6]

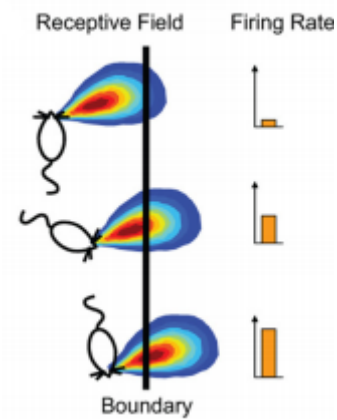


Figure 2.3.: Similar to 2.2 an illustration of a receptive field in allocentric coordinates. Dark red indicates the cell's tuning location. When a boundary is at the centre of the cell's receptive field the cell reaches it's peak firing rate. The cell's firing gradually increases with the boundary coming closer to the receptive field's centre.[18]

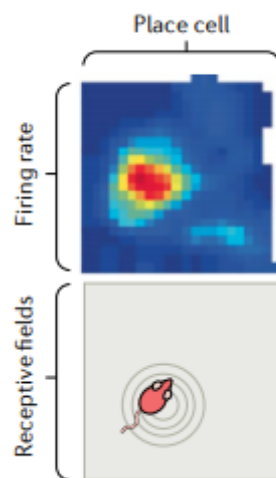


Figure 2.4.: When the animal is at a certain location a place cell fires. (Top) Firing rate depending on the animal's location, and the bottom image shows the receptive field. [6]

2.2. Biological properties of Head Direction Cells

Each Head Direction Cell is tuned to a specific allocentric heading direction, and reaches its peak firing rate when the agent is facing in that particular direction. The specific direction where the cell's response is at its peak is referred to as the cell's preferred firing direction. This characterization is described by the cell's tuning curve, which is Gaussian in shape. There are two ways for HDCs to get their information: Landmark navigation and path integration. When using landmark navigation the animal derives its current orientation relative to surrounding landmarks. In path integration the animal uses self-movement information to maintain the cell's functioning. Most of the time both processes are used and integrated simultaneously [30]. For example when its completely dark the animal has to rely solely on path integration. In an experiment a rat was put in an environment with a card as the only cue for navigation. After putting the cue card in a different place the HDC's preferred directions changed by the same amount [29]. This experiment shows that the HDC's orientation is also anchored to external hints.

3. Related Work

Bicanski and Burgess model of spatial memory and imagery is the only neural-network-based model that incorporates egocentric and allocentric representations as well as transformation between them, in the neuroscientific landscape [19]. Thus, their model serves as the guideline for the model proposed here.

3.1. BB-Model of spatial memory and imagery

The neural level model of spatial memory and imagery by Bicanski and Burgess (BB-Model) is a theoretical model that tries to explain how neural representations of egocentric spatial experiences in parietal cortex interface with viewpoint-independent representations in medial temporal areas, via retrosplenial cortex, to enable many key aspects of spatial cognition [5].

The BB-Model builds upon the work of Byrne, Becker and Burgess [8], [9]. The essence of the model is transforming egocentric representations of the local environmental surroundings (objects and boundaries) into allocentric representations for long-term storage, supporting imagery and recollection. For that multiple neuronal populations found in Papez' circuit, parietal, retrosplenial and medial temporal areas are modeled. From the Medial Temporal Lobe (MTL) that includes PCs, HDCs, GCs and BVCs.

The neurons coding for the presence of objects and boundaries in the egocentric space reside in medial parietal cortex. In the model they refer to it as the parietal window (PW). The PW contains two neuron populations one coding for boundaries (PWb) and one coding for discrete objects (PWo). The transformation from egocentric to allocentric reference frame is performed by a gain-field circuit in retrosplenial cortex. Gain modulation is a nonlinear process of neurons combining information from two (or more) inputs, which may be of sensory, cognitive or motor origin. When one input (the modulatory one), has influence on the gain or sensitivity of the neuron to the other input, without modifying its selectivity or receptive field properties, it is called gain modulation [25].

Here the gain modulation is provided by head-direction, producing directionally tuned BVCs and OVCs (Object Vector Cells - allocentric analogues to BVCs coding for discrete objects) which connect egocentric and allocentric coding neurons.

BVCs and OVCs are part of the medial temporal lobe network for spatial context. The MTL network consists of three interconnected neuron populations. BVCs (and OVCs) and PCs code for the position of the agent relative to boundaries and objects, and perirhinal neurons which code for the identity (color, texture, etc.) of boundaries (PRb) and objects (PRo). OVCs and BVCs only code for location, perirhinal PRbs and PRos for the identity of boundaries and objects.

BVCs and OVCs are reciprocally connected to the transformation circuit. Connections within the MTL network form an attractor network (an attractor network is a network that evolves toward a stable pattern over time), such that mutual excitatory connections between neurons ensure pattern completion. Thus, if the network is partially stimulated in any neuron population, previously learned representations of spatial context are re-activated.

The Model has two modes of operation: bottom-up and top-down. During bottom-up mode, which is analogue to perception, the transformation circuit maps egocentric to allocentric representations and thus determines MTL network activity. During top-down mode the circuit acts in reverse. It does so to reconstruct the egocentric from the allocentric representation, to form the groundwork for allocentric memory. For mental navigation and planning they include a grid cell population which drives sequential place cell firing. Mental navigation meaning imagined movement through a known environment. Figure 3.1 illustrates the BB-Model's schematic as described above.

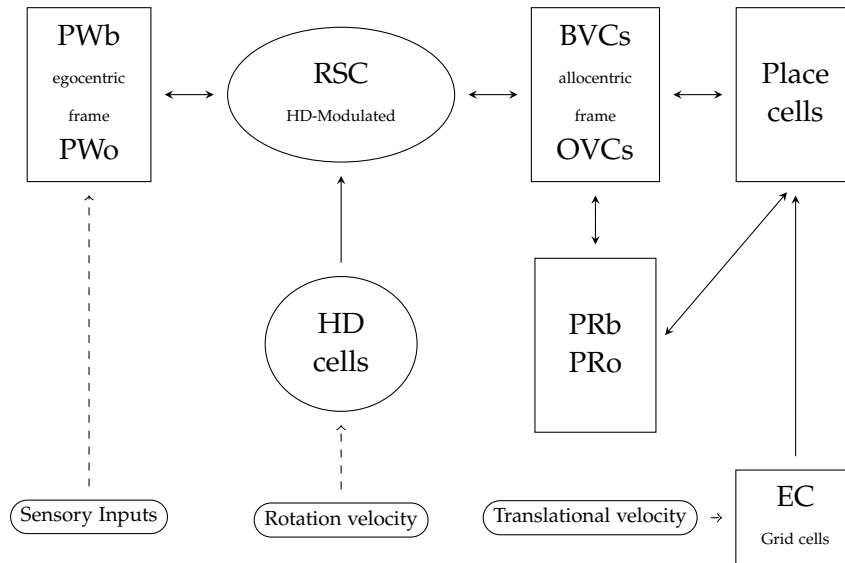


Figure 3.1.: Schematic of the BB-Model as described in section 3.1. Sensory inputs, rotation velocity and translational velocity are provided by the agent [5].

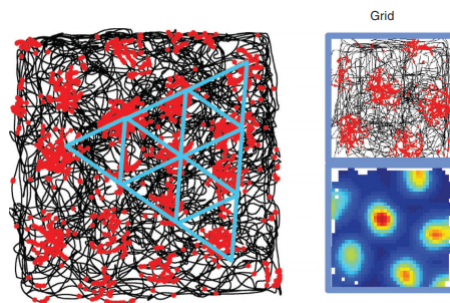


Figure 3.2.: Recording from a rat brain which shows how a grid cell is firing. (Left) The black trace shows the trajectory of a foraging rat in a square enclosure. Red dots are spike locations of the grid cell. Blue equilateral triangles have been drawn on top of the spike distribution to illustrate the regular hexagonal structure of the grid pattern. (Right) On the top is the same as on the left. The bottom is a color coded rate map with red showing high and blue showing low activity. [20]

4. Methodology

The model combines ideas from the BB-model of spatial memory and imagery by Bicanski and Burgess [5] with Amir el Sewisy's HDC network. In this chapter, the neuron model is defined in section 4.1. After that the HDC and BC networks architecture are introduced in sections 4.2 and 4.3. Then it is explained how the synaptic weights connecting the different components are generated in section 4.4. Lastly, how perception is performed during simulation, is specified in section 4.5.

4.1. Neuron Models

4.1.1. Boundary Coding Neurons

The Model uses rate-coded neurons. The activation function consists of two gaussians which are multiplied with each other. One is tuned to the distance and the other to the direction at which a specific boundary is located at in relation to the agent.

Each boundary cell i is tuned to specific coordinates (p_i, ϑ_i) (polar coordinates). If the coordinates of a boundaries location are (p, ϑ) , then the activity of each boundary selective cell is proportional to the distance of its receptive field from that boundary segment. The following equation calculates the firing rate r for the i -th boundary coding neuron:

$$r_i = \frac{1}{p} * \exp\left(-\left(\frac{\vartheta_i - \vartheta}{\sigma_\vartheta}\right)^2\right) * \exp\left(-\left(\frac{p_i - p}{\sigma_p}\right)^2\right) \quad (4.1)$$

Where σ_ϑ and σ_p define spatial dispersion of the rate function r . $\sigma_\vartheta = 0.2236$ is a constant which describes the cells angular tuning width, and σ_p is a variable parameter that describes a cells sensitivity in terms of distance. This varies in a linear way with distance. Cells with a preferred firing distance further away from the agent have wider firing fields [18]. σ_p is described by the following equation:

$$\sigma_p(p_i) = (p_i + 8) * 0.08 \quad (4.2)$$

4.1.2. Head Direction Cells

During training, which will be described in section 4.4 each HDC's activity f_i is calculated using a gaussian function described by Equation 4.3.

$$f_i = \exp\left(-\left(\frac{\theta_i - \theta}{0.125}\right)^2\right) \quad (4.3)$$

with θ being the current heading direction and θ_i being neuron i 's preferred heading. The reason to use a simple gaussian is because actual HDCs resemble a gaussian bell curve[30], and it follows all the properties that will be defined in section 4.2. Additionally in the HDC model a single neuron's activity is dependent on the previous state, i.e. it is time dependent. During training, no time dependency is needed to set up the weights. This will be explained in the following sections.

The HDC's neuron model for simulation is taken entirely from Amir El Sewisy's bachelor thesis. This neuron model is used during simulation to decode real-time heading direction. In his network Amir uses a neuron model inspired by [22]. The model uses firing rate for computation of neuronal activity, and was selected because it was built using in-vivo data recently recorded. For each neuron i , there is a variable f_i describing its firing rate. All f_i are initialized with 0 and their behaviour over time is described by the differential Equation 4.4

$$\tau \frac{df_i}{dt} = -f_i + \phi\left(I_i + \sum_j w_{ij} f_j\right) \quad (4.4)$$

τ is the time constant, its value is re-used from [22] and defined in Table 4.1. w_{ij} is the synaptic strength, also referred to as synaptic weight, from neuron j to neuron i . Excitatory synapses are modelled with positive weights and inhibitory synapses are represented with negative weights. I_i is the external input current from outside the network to neuron i . $\phi(x)$ is called the single-neuron transfer function and is defined in Equation 4.5 [22]:

$$\phi(x) = \frac{r_m}{1 + \exp(-\beta_t(x - h_0))} \quad (4.5)$$

ϕ is a sigmoid function, its parameters r_m , β_t and h_0 were inferred to fit data recorded from in-vivo neurons by [22] and are re-used in the HDC network simulation, See Table 4.1. $\phi(x)$ is visualized in Figure 4.1. Following Equation 4.4, the firing rate of a neuron with constant external and synaptic inputs x converges to $\phi(x)$ over time. Note that $\phi(x) \approx 8.95$, which means that an isolated neuron fires with a rate of about 8.95 Hz without any external input. The maximum firing rate is $r_m = 76.2$ Hz, which is the upper bound of $\phi(x)$.

r_m	76.2	Hz
β_t	0.82	
h_0	2.46	
τ	20	ms

Table 4.1.: Model parameters, re-used from [22]

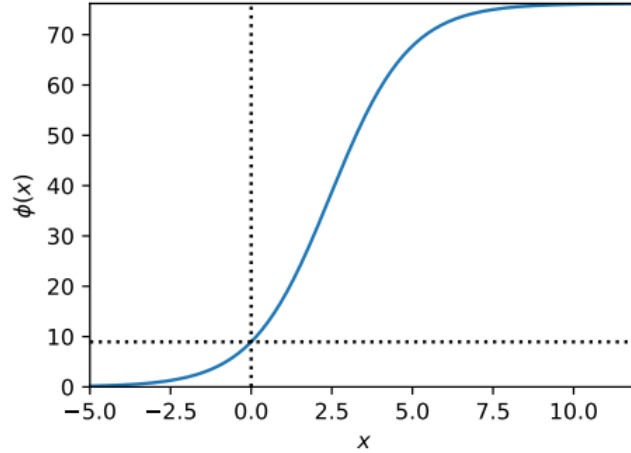


Figure 4.1.: The single-neuron transfer function $\phi(x)$ defined in [22]

4.2. HDC Network Architecture

In this section the HDC network's basic architecture will be explained, a more detailed description of all the different components can be found in Amir El Sewisy's work.

The network consists of $n = 100$ HDCs. The HDC's preferred directions θ_i with $i \in \{0, \dots, n - 1\}$ are equidistantly spaced over 2π radians. The neuron indexed with 0 has the preferred direction $\theta_0 = 0^\circ$ and the preferred directions are assigned to neurons in counterclockwise order. Thus, neuron i has preferred direction $\theta_i = \frac{2\pi}{n}i$. The activity of each neuron in the HDC network plotted over their preferred directions is referred to as the HDC network's activity profile.

Each HDC's activity is governed by the head direction, the mapping of head direction to a HDC's activity is called its tuning curve. $\Omega_\theta(\alpha)$ is defined as the activity of the HDC with preferred direction θ while the head is facing in the direction α , i.e. its tuning curve evaluated at α . When the head is facing at direction α the network's activity profile resembles the tuning curve of the single HDC with preferred direction α .

The HDC network's activity profiles have to be stable over time, i.e. the activity profile at timestep $t + 1$ has to be the same as the one at timestep t , if there is no

external stimulus that causes the activity profile to change. This stability is achieved by an attractor topology.

To form a stable activity peak, neurons close to each other are connected by excitatory synapses while neurons further away are connected by inhibitory synapses. Initially, there is no activity in the network. If a single neuron or a group of close neurons receives an outside stimulus, the stimulated neurons in turn stimulate close neurons due to the local excitatory synapses. Neurons further away from the initial stimulus are instead inhibited by the group of active neurons due to the global inhibitory synapses. The synaptic weights are chosen such that the initial stimulus results in a stable activity peak around that stimulus, i.e. the activity peak is maintained after removing the initial stimulus.

The initial stimulus will result in a stable activity peak at 0° . Afterwards the external stimulus that will shift that activity peak is angular velocity.

4.3. BC Network Architecture

The architecture is derived from the BB-Model of spatial memory and imagery [5].

4.3.1. Activity Profile

The activity profile of the network is each neurons activity plotted with respect to their specific boundary tuning. All neuron's activities plotted together is referred to as the BC network's activity profile. As stated before each neuron is tuned to a specific distance and angle at which a boundary segment can be encountered. The tuning curve follows a 3-Dimensional bell curve. In addition with increasing distance of the boundary, the tuning width with respect to distance of a neuron, gets bigger. This is consistent with recordings made in rat brains where BVCs that react to boundaries further away from the rat have broader receptive fields than those which react to closer boundaries[18]. At each time step the activity profile is computed as follows: For each boundary segment present in the environmental surrounding, the firing rate of each individual neuron is calculated according to equation 4.1. Afterwards each neurons activities with respect to all the segments are added together. Lastly, the activity of all neurons will be normalized to one.

The activity profile is illustrated by arranging all eBC and BVC neurons, according to the relative locations of their receptive fields (see Figure 4.4). When taking a snapshot of the neuron population of either eBCs, transformation layers or BVCs, that snapshot will then give a representation of the current sensory environment (see Figure 4.3). In the human's, or a rodents brain the neurons are probably not physically organized the same way, but for the sake of visualization and since it does not hinder performance

in this model this topology is used. Population snapshots are distinct from firing rate maps (see Figure 4.2) which show, at which location in an environment a specific neuron is firing.

The receptive fields are distributed on a polar grid, with individual receptive fields centered on each tile. As an example, 16 receptive fields (computed by Equation 4.1) are overlaid (bright colors) on the polar grids for illustration (see Figure 4.4). Note that each receptive field covers multiple tiles, that is neighboring receptive fields overlap. The polar grids of receptive fields tile the space around the agent (white circle at center of plots), and they are anchored to the agent moving with it (for both BVCs and eBC neurons). In addition, for eBC neurons the polar grid of receptive fields also rotates with the agent (i.e. their tuning is egocentric).

The radial separation of distance bins (see Figure 4.4) increases linearly from 0.21 to 1.71 along the radius of length 16 distance units. The receptive fields of BVCs, eBC neurons and retrosplenial cells (transformation layers) tile the space in polar coordinates with a radial resolution of 1 receptive fields per arbitrary distance unit (range: 0 – 16, see above) and an angular resolution of 51 receptive fields over 2π radians, which results in a total of 816 neurons per population.

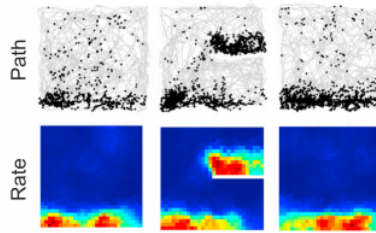


Figure 4.2.: Rate maps recorded in-vivo. On the top the black dots along the trajectory indicate spike locations of single neurons. Below the corresponding rate maps are illustrated [7].

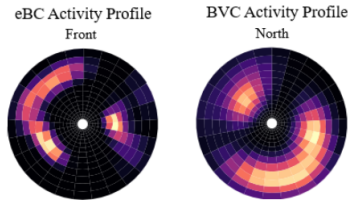


Figure 4.3.: Activity profiles of eBC (left) and BVC (right) layers at the same time during simulation. All the neurons are arranged as described in section 4.3.1. Bright colors indicate a higher firing rate. Environmental surroundings are visualized by neuronal firing.

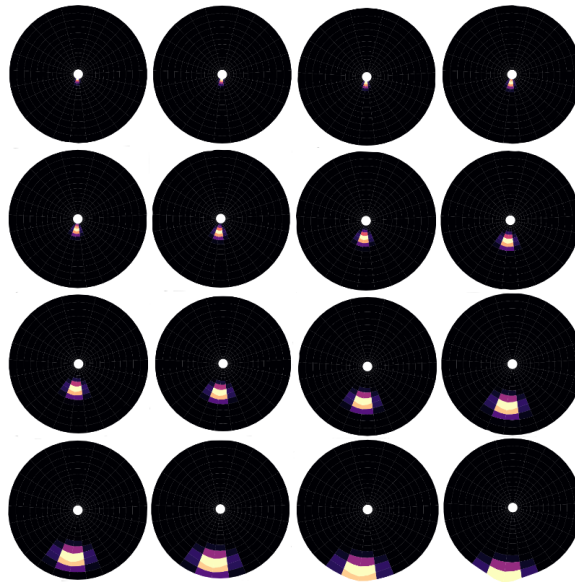


Figure 4.4.: Sixteen receptive fields along the 16 distance units. The closer to the agent the smaller the receptive field. The receptive fields shown here are all located on the same radian. The top left shows the receptive field closest to the agent and in the bottom right the receptive field furthest away from the agent is shown. Bright yellow indicates a higher firing rate (calculated according to Equation 4.1).

4.3.2. Architecture

This thesis only differentiates between egocentric and allocentric reference frames. Nevertheless the first reference frame of visual information is the retina. So there has

to be another transformation taking place, which transforms the eye centered signal into a head centered representations, and then drives the BCs to fire [6]. However this thesis focuses on what happens after these measures are obtained.

51 sensors are used to scan the environment, to get distances and directions to all boundary segments at a given time step. From that the egocentric activity is calculated.

Once the egocentric activity is calculated the activity is propagated to the 20 transformation layers belonging to the transformation circuit. This happens by multiplying it with 20 weight matrices which are obtained according to the hebbian learning rule which is explained in section Synaptic Weights. These transformation layers are then subject to modulation by the HDC network. Depending on the current heading direction provided by the HDC network, the transformation layer matching the current heading will be propagated to the BVC layer. As long as the HDC signal is modelled as a gaussian (which is biologically plausible) [8], [9], [5] show that 20 layers guarantee enough overlap to succesfully interpolate between the maximally effective head directions [6]. In the following the transformation circuit will be described in more detail.

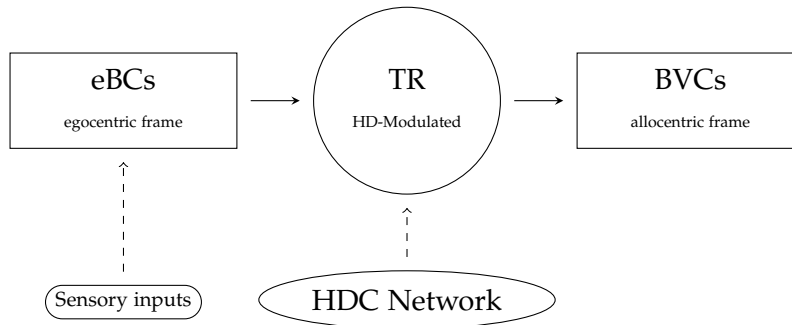


Figure 4.5.: Model schematic as described above in section 4.3.2

4.3.3. Transformation Circuit (TR)

The TRs task is to transform head-centered (egocentric) perceptual information into an allocentric reference frame. Our sensory information is, at the first step, of egocentric nature (after transforming the retinal representation as previously mentioned) i.e., in the context of boundary detection, a boundary is either ahead, left or right. This egocentric information is transformed into an allocentric reference frame by a gain-field circuit in retrosplenial cortex. The gain modulation is provided by head-direction, producing directionally tuned boundary vector cells (BVC) which connect egocentric and allocentric boundary coding neurons.

Here the HDC being the modulatory cell is influencing the BVC firing. The same

eBC can drive multiple different BVCs to fire depending on heading direction (HDC input modulates effect of eBC input to BVC firing).

For example, an eBC with a receptive field (RF) to the right while moving west connects to the BVC coding for allocentric north, an eBC with its RF to the left while moving east is connected to the same BVC (see Figure 4.7). Likewise an eBC with a receptive field to the right is connected to multiple BVCs depending on the heading direction of the agent.

The TR consists of 20 identical sublayers, each tuned to a specific heading direction. Each subpopulation encodes a rotated egocentric map, representing its heading direction chosen from 20 evenly spaced allocentric heading directions from the 360° range. Connections between the eBC layer and any one of the transformation sub-populations are set up in training in such a way, that a rotated version of the egocentric spatial information contained in the eBC is projected onto that transformation sublayer (details in section 4.4).

Weights from the HDC network to the transformation layers are set up in such a way that all transformation layers that do not match the current heading are inhibited, and those that do represent it remain active, and thus propagate their activity profile to the BVC layer (Figure 4.6). This is achieved by scaling each Layer's activity with respect to angular difference between the current heading and the directional tuning of that specific layer, i.e. the bigger the angular difference the smaller the remaining activity of the layer. Afterwards all the layers activities are added together, and normalized to one. The result is the transformation from a perceived egocentric environmental surrounding into an allocentric representation.

E.g. if the agent has a wall in front of him (0° in egocentric coordinates) each of the 20 layers will have that information but rotated in such a way that it represents their specific tuning (e.g. 90° : allocentric west , 180° : allocentric south, 270° : allocentric east). If the agent is heading east (270°), only the layer representing that heading will be able to project onto the BVC layer, and therefore the BVC will represent a boundary in the allocentric east (see figure 4.6).

4. Methodology

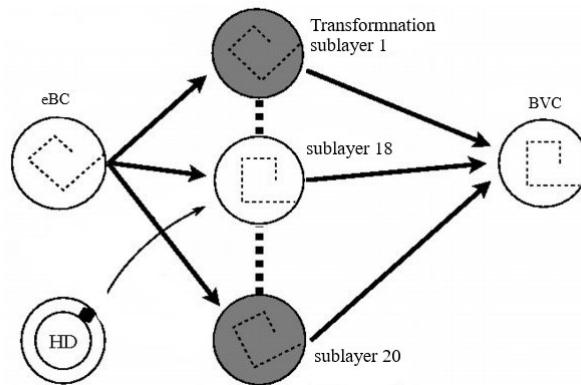


Figure 4.6.: Egocentric boundary information is shown in the eBC layer. The sublayers each encode the same egocentric map, but rotated. For simplicity only three sublayers are shown here. With heading direction at approx. 322° , sublayer 18, which is tuned to approximately 322° , is the layer which represents the current heading direction. The activity profile of sublayer 18 is then projected to the BVC layer while the others are inhibited[18].

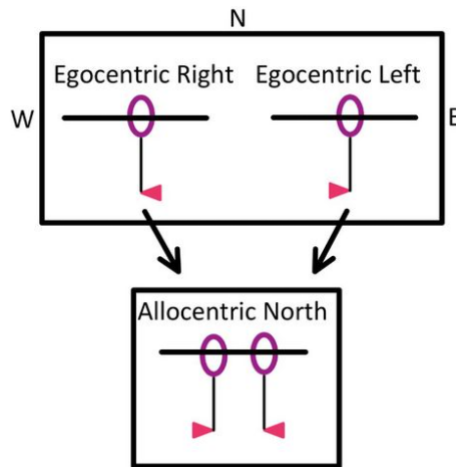


Figure 4.7.: Neurons with receptive fields to the right and left in the egocentric reference frame are both connected to the same BVC in the allocentric reference frame.

4.4. Synaptic Weights and Training

During training phase all the synaptic weights that connect the different components of the model are set up. The training phase follows the same steps for 400.000 iterations:

A random boundary segment is generated in allocentric coordinates, and the corresponding firing rates for the BVCs are calculated according to Equation 4.1 resulting in the BVC's activity profile.

Afterwards the boundary segment is rotated and the corresponding activity profiles for the egocentric and transformation layers are calculated (also according to Equation 4.1). In the next section I will explain how the synaptic weights are generated from those activity profiles.

4.4.1. Synaptic Weights

The underlying principle is the "Hebb rule":

Connections between neurons increase in efficacy in proportion to the degree of correlation between pre and post-synaptic activity [15]. Meaning, if pre-synaptic neuron *A* excites post-synaptic neuron *B* the connection between those two is strengthened and firing of neuron *A* will most likely lead to the firing of neuron *B*. The more often that happens the stronger the connection between *A* and *B*. Or with Hebb's words "Neurons that fire together, wire together".

Following that principle the connection weights are calculated using the outer product of two vectors. The reason the outer product is the fitting operator is because it multiplies each element (representing a neurons activity in this case) of one vector with each element of the other vector, which is fitting to Hebb's rule.

$$eBC \text{ to } TR: \quad \underset{816 \times 816}{\text{egocentric2transformation}} = \underset{816 \times 1}{eBCActivity} \times \underset{1 \times 816}{TRlayer'} \quad (4.6)$$

The weights connecting the eBC and each of the 20 TR layers is the outer product of the corresponding activity profiles. So in total the weight tensor that connects the eBC layer to all 20 TR layers is $816 \times 816 \times 20$ in size. This is done repeatedly for all of the 400.000 iterations, in order to account for learning all different places a boundary can be encountered at. After each iteration the weights calculated will be added to the previous weights, and after iterating 400.000 times the weights will be normalized to one.

$$HDC \text{ to } TR: \quad \underset{816 \times 100}{\text{heading2transformation}} = \underset{100 \times 1}{HDCActivity} \times \underset{816 \times 1}{TRlayer'} \quad (4.7)$$

The weights connecting the HDC network and the TR layers are calculated the same way. 20 weight matrices resulting in a $816 \times 100 \times 20$ weight tensor are calculated with the outer product of the HDC's activity profile and the corresponding TR layer's activity profile. This is only done once per Layer since the directional tuning per layer does not change.

As stated previously connection weights from TR to BVC are the identity matrix since it just conveys the TR's outcome, so there are no computations needed for those.

Once the weights are calculated they are saved and can be used in the simulation or any real-time application, if the environmental surroundings are put in with the right format (Vector with 816 elements).

4.5. Perception

During simulation (or possibly any real-time application) the agent needs to get information about the environmental surroundings, and the allocentric heading direction. Here environmental surroundings are scanned by 51 sensors distributed around the agent (see Figure 5.1, and the heading direction is calculated by the HDC network provided by Amir El Sewisy. 51 sensors are used because there are 51 receptive fields per distance unit aligned around the agent. The information about the environmental surroundings is fed into the eBC layer and the activity profile is generated (Equation 4.1). The HDC network provides gain-modulation for the TR, and the information propagates through the network generating BVC activity.

As explained in section 4.3.1, the model encodes distance with $d = 16$ distance units. The sensors used in the simulation have a length of $l = 2.5$. So the distances to the boundaries have to be rescaled to fit the model. The rescaling factor k can be computed with following equation:

$$k = \frac{d}{l} \tag{4.8}$$

By doing this, it is possible to use the same simulation environment, for simulating wider or narrower spaces. This can be done by adjusting the sensor length. The longer the length, the smaller the space appears. And vice versa, the shorter the length, the bigger the space appears (Figure 5.14).

5. Results and Discussion

In this chapter the different simulation settings will be described first, and then the results of the simulations are discussed. Afterwards firing rates of eBC and BVC populations are compared. Finally biological plausibility of the model is debated.

5.1. Simulation Setup

The firing of boundary coding cells is tested by getting environmental information from a simulated pioneer P3DX robot. The environment is running in PyBullet3 [10]. The robot is controlled by a braitenberg controller that avoids obstacles based on proximity, and is equipped with 51 proximity sensors as shown in Figure 5.1.

Those sensors provide input to the braitenberg controller, and to the egocentric eBC layer of boundary coding neurons. Thus, as said those sensors are simulating perception.

The robot's angular velocity is the input for the HDC network, which encodes current heading direction and provides gain-modulation for the transformation circuit. The robot enters two of the maze's versions on the bottom right see Figure 5.2 and Figure 5.3 and one at the bottom left see Figure 5.4. Afterwards the robot will navigate through those mazes.

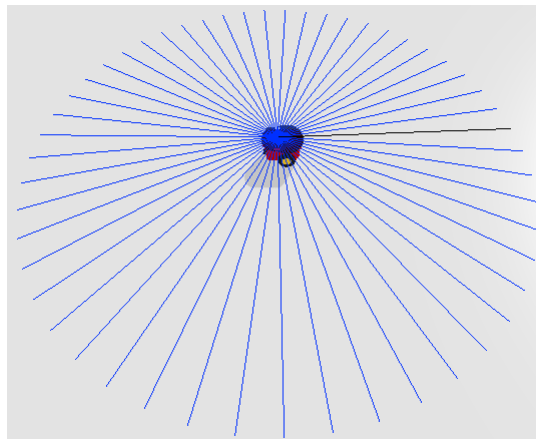


Figure 5.1.: Pioneer P3DX equipped with 51 proximity sensors.

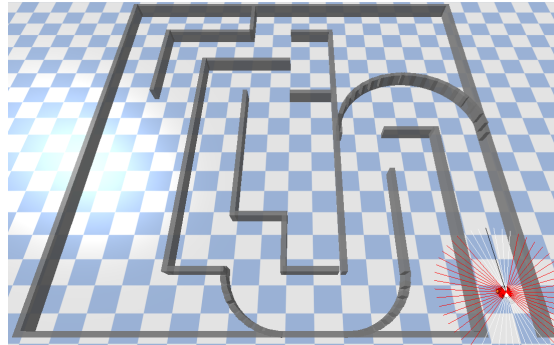


Figure 5.2.: Simulation environment: maze with round turns

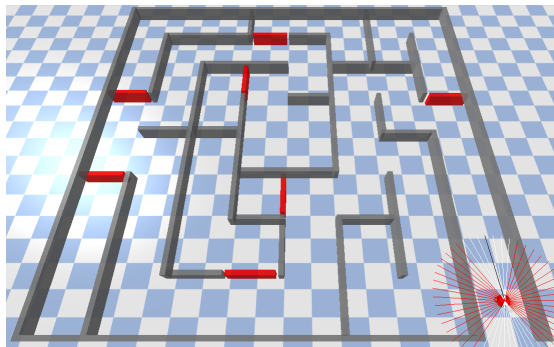


Figure 5.3.: Simulation environment: maze

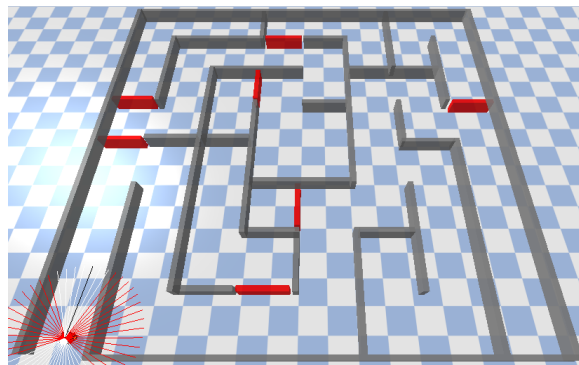


Figure 5.4.: Simulation environment: Maze with entry on the bottom left

5.2. Simulation Results

During simulation the different layer's activity profiles are plotted for visualization. We will use the plotted activity profiles to discuss the applicability of the model and how good it works (see Figures 5.5 - Figure 5.16). The BVC layer's activity profile is depending directly on the HDC network's decoded direction. Thus if there is an error in the decoded direction it is represented in the BVC layer. The maximum error, as reported by Amir El Sewisy, is 1.5° .

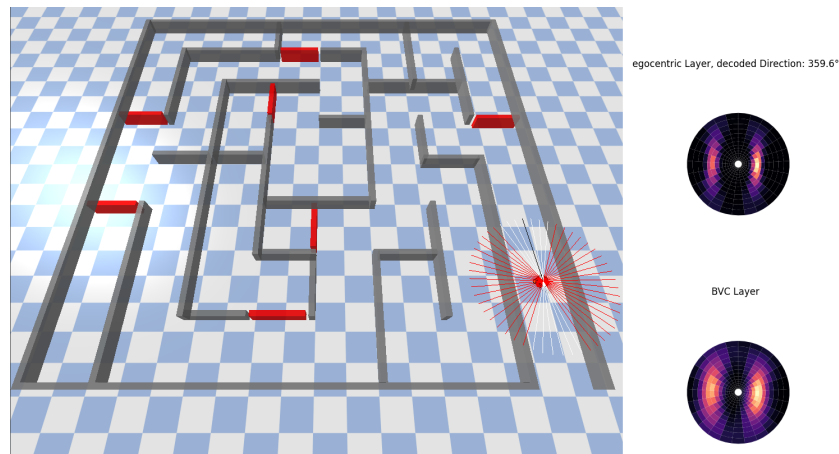


Figure 5.5.: The agent is facing a decoded direction of 359.6° which is allocentric north. In the agent's peri-personal space there are walls left and right. The result is that the BVC and eBC activity profiles are approximately the same.

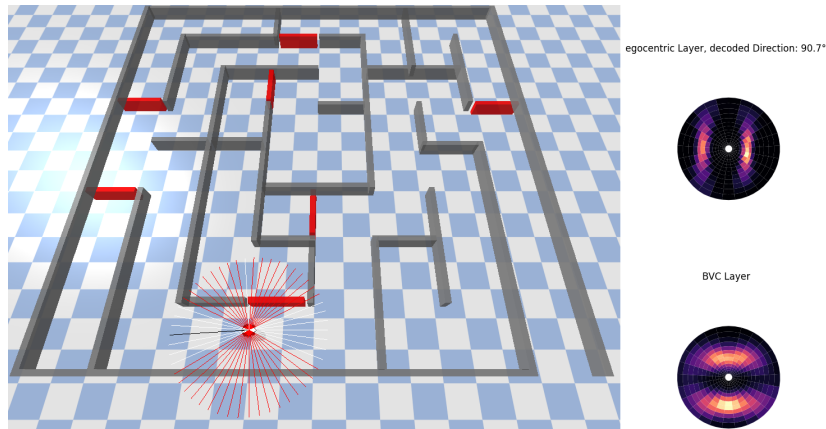


Figure 5.6.: The agent is facing a decoded direction of 90.7° which is allocentric west. In the agent's peri-personal space there are walls left and right, so the same as in figure 5.5. The transformation circuit rotates the representation by 90° and propagates that to the BVC layer, to produce allocentric representation in the BVC layer.

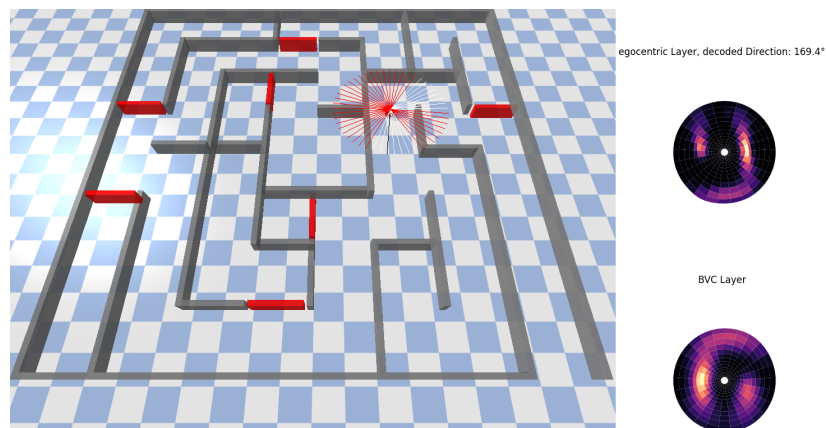


Figure 5.7.: The agent is facing a decoded direction of 169.4° which is allocentric south. In the agent's peri-personal space there are walls left, right and behind. Due to the sensors being distributed all around the agent, the wall behind him is represented in the activity profile as well. This is only biologically plausible to some extent. It is expected that there is a mnemonic component involved that gives rise to BCs with a receptive field behind the agent. However this firing is like the agent has a 360° field-of-view. Discussed more in section 5.4.

5. Results and Discussion

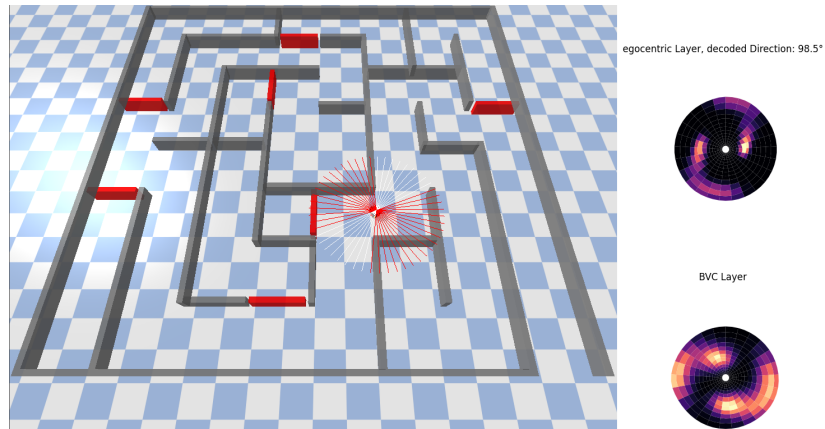


Figure 5.8.: The agent is facing a decoded direction of 100.6° which is allocentric west. In the agent's peri-personal space there are walls left, right, behind and in front of him producing a S like turn.

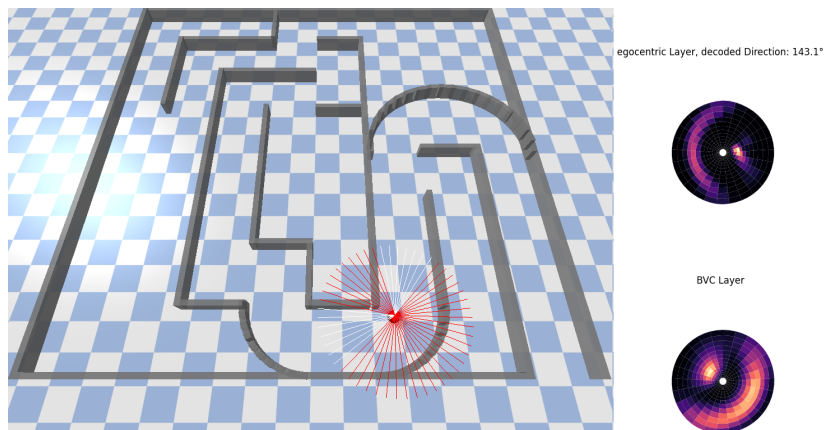


Figure 5.9.: The agent is facing a decoded direction of 143.1° which is allocentric south-west. In the agent's peri-personal space there is a corner to the right, and a curved wall to the left. This scenario shows that the model is able to produce egocentric and allocentric firing that reflects curved surroundings.

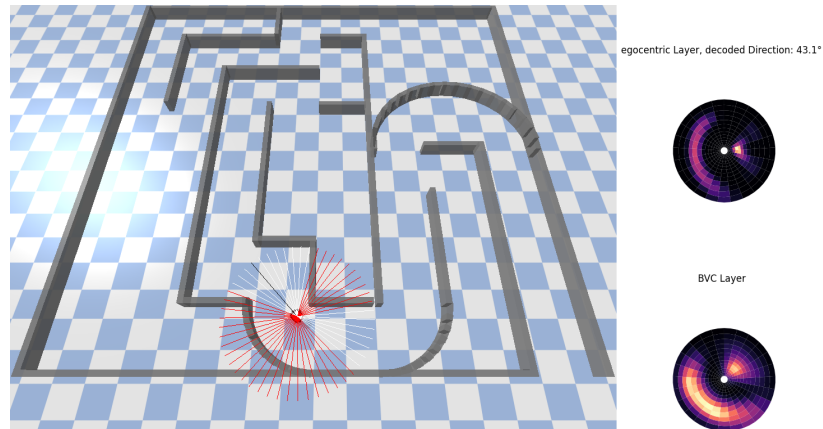


Figure 5.10.: The agent is facing a decoded direction of 43.1° which is allocentric north-west. In the agent's peri-personal space there is a corner to the right, and curved wall to the left. It is almost the same scenario as above in figure 5.9, but with a different heading.

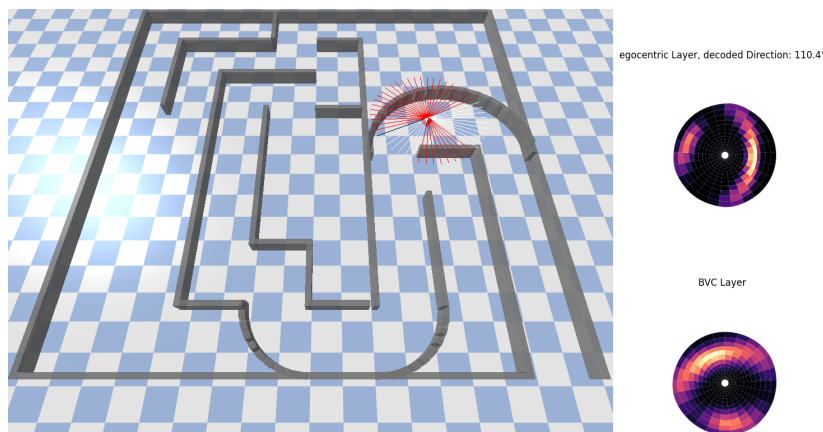


Figure 5.11.: The agent is facing a decoded direction of 110.41° which is approx. allocentric west. In the agent's peri-personal space there is a curved wall revolving around him from behind-right to front-right. To his left is a short wall. Different to scenarios 5.9 and 5.10 the wall is now to the right in a left turn. Both egocentric and allocentric produce accurate activity profiles.

5. Results and Discussion

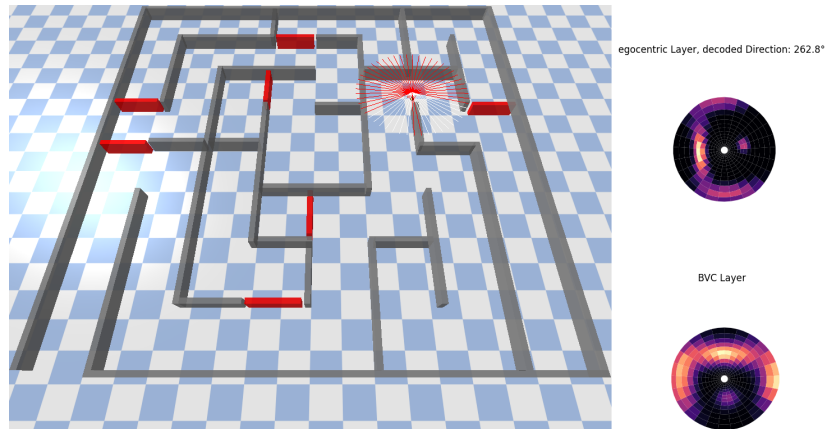


Figure 5.12.: The agent is facing a decoded direction of $262.8.0^\circ$ which is allocentric east. In the agent's peri-personal space he is surrounded by walls behind, left and in front of him, to his right there is the edge of a wall. Different from the other scenarios the agent is now moving east. The transformation circuit works just as good as while moving west and produces accurate BVC firing.

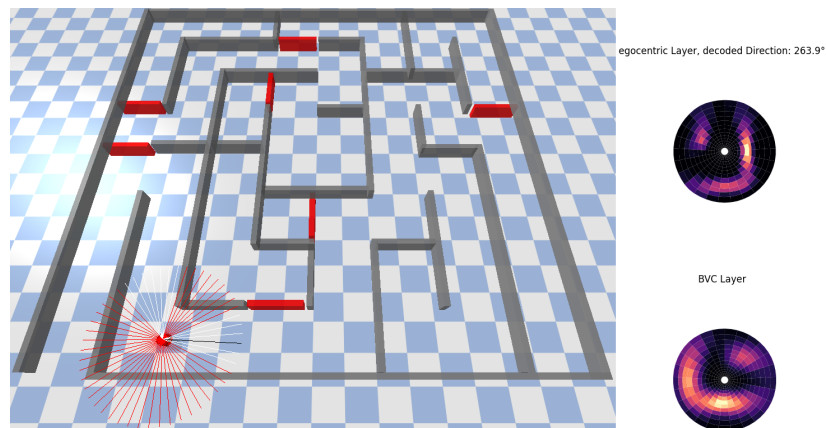


Figure 5.13.: The agent is facing a decoded direction of 263.9° which is allocentric east. In his peri-personal space there are walls left, right and behind. Another scenario to show the transformation circuits functioning for heading east.

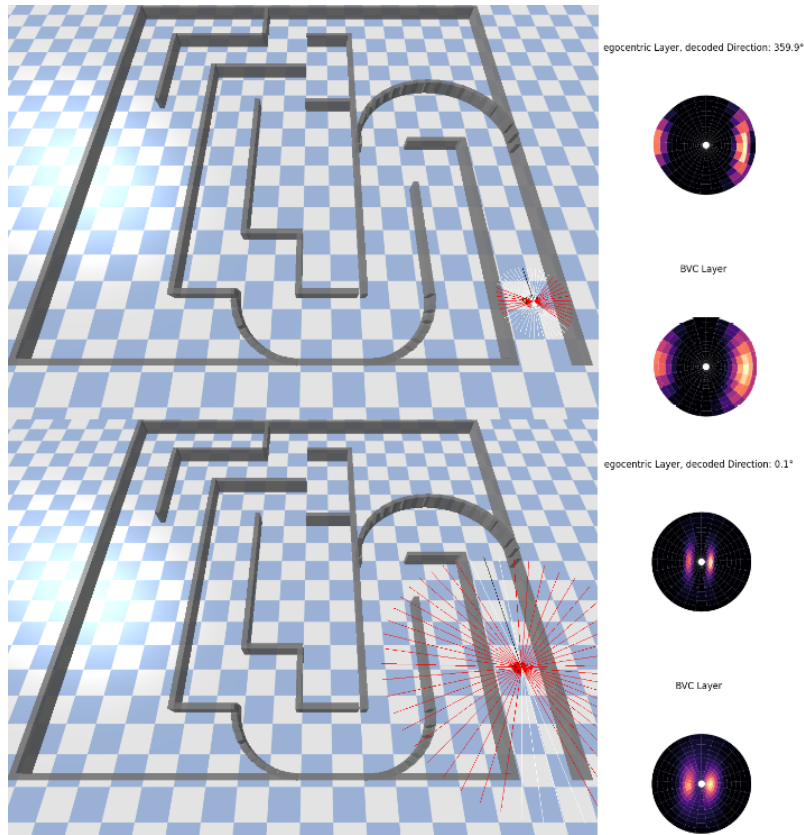


Figure 5.14.: The agent is facing a decoded direction of 359.9° on the top and 0.1° on the bottom which is both allocentric north. In both Simulations the agent is in between two parallel walls. Normally the sensor length is 2.5. On the top the sensor length is halved to be 1.25 and on the bottom it is doubled to be 5. The result is, as described above in section 4.5, a change in how the environment is perceived in terms of space. On the top space seems wider, and on the bottom it seems narrower.

5. Results and Discussion

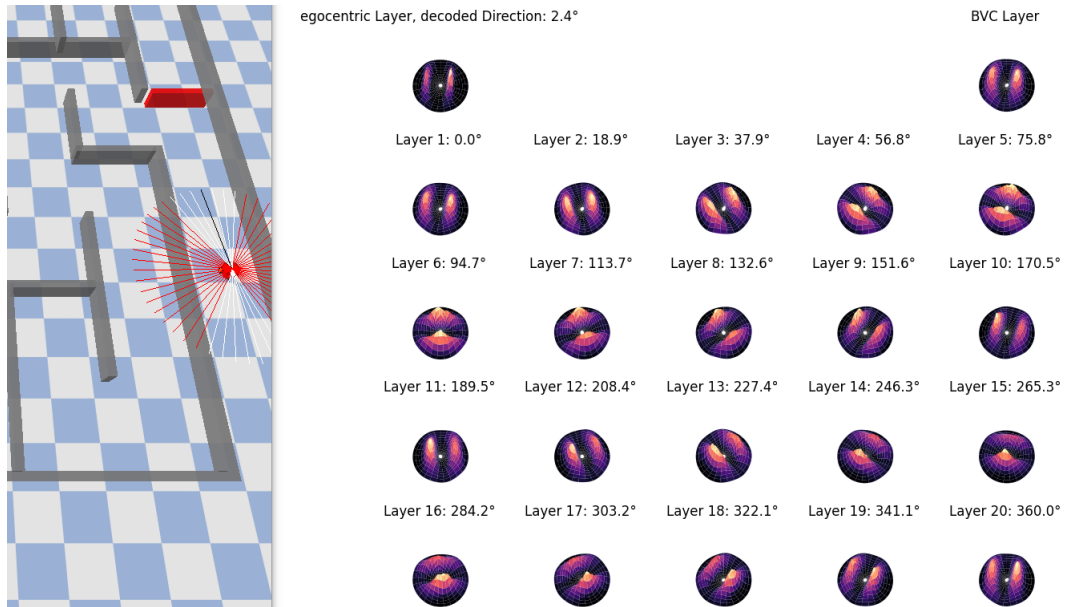


Figure 5.15.: The agent is facing a decoded direction of 2.4° which is allocentric north. In his peri-personal space there are walls left and right. This is the same as in Figure 5.5, but with all 20 transformation layers plotted. It shows the counter-clockwise rotation of the eBC's activity profile through layers 1 to 20.

5. Results and Discussion

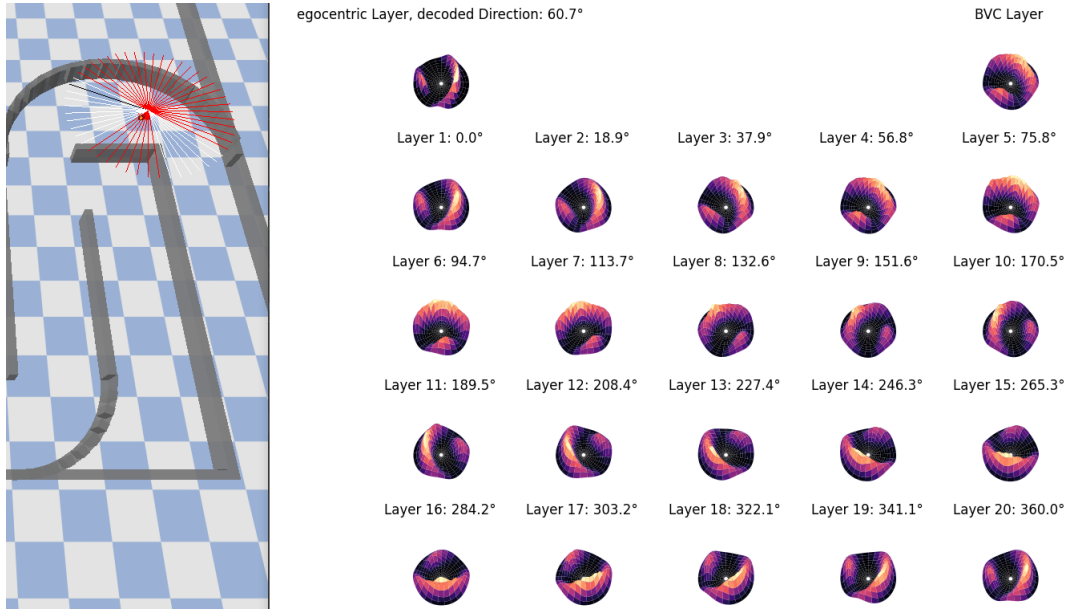


Figure 5.16.: The agent is facing a decoded direction of 60.7° which is allocentric north-west. In his peri-personal space the surrounding environment is similar to Figure 5.11. Again all 20 transformation layers are plotted, and the figure shows the counter-clockwise rotation of the eBC's activity profile through layers 1 to 20. All the 20 layers represent the curvature of the wall to the right/allocentric north.

All those different simulation scenarios show that the BC network works as it is supposed to. The plotting of the activity profile shows that the neuronal firing represents the environmental surroundings. It works for corners, and for curved walls as well. While facing in all different allocentric directions and at the same time encountering surroundings, which are very similar in the egocentric reference frame, the transformation circuit conducts the transformation in such a way that the encoded environmental surroundings are represented accordingly in the allocentric reference frame. The only difference that stands out is that, although allocentric firing properly displays the environmental surroundings accordingly and the transformations work as well, the difference in size of firing fields of the populations are apparent. This will be evaluated in the next section.

5.3. Rate Differences

Here I will compare the sum over the neuron's firing rates from eBC and BVC populations in the regular maze environment (see figure 5.3) and the maze with curved turns (see figure 5.2). Simulation episode for the regular maze is 240s and 180s for the maze with curved turns.

The eBC will serve as ground truth. The reason for that is that the input (distances and directions to environmental surroundings) to the eBC layer is scanned by sensors and by that, is 100% accurate. The neuron model is biologically plausible and the activity profile is computed according to neuroscientific evidence as well [5], [9].

All neurons firing rates have been normalized to one throughout the model. This means that relative firing rates are accurate, but peak firing rates with respect to biological evidence differ. This has no influence on performance, because any arbitrary peak firing rate r could be simulated by multiplying all the activity with that arbitrary rate r . But it would not change the model's outcome. This means that if all neurons of a population would be firing maximally the total rate would be 816, since each population consists of 816 neurons.

Between all simulation environments the maximum firing rate difference is 125.70, the mean rate difference is 79.08, the maximum eBC rate is 66.56 and the maximum BVC rate is 172.27. Looking at the trajectory, differences and where the robot was located at different time steps it shows that the difference is the biggest when there are more boundary segments located on receptive fields of the neurons. (see figures 5.17, 5.18, 5.19).

Comparing the values with the maximum value differences between eBC and one of the transformation layers (TR layer 6 was chosen randomly) (see figure 5.20) with mean difference = 62,79 and maximum firing difference = 98.73, shows that those values are smaller than in comparisons between eBC and BVC. This implies that each propagation step adds to the loss of accuracy. It has to be differentiated where the loss comes from:

- *eBC to TR*: The weights are generated using the outer products between eBC and TR layers. Rotation from eBC to TR layers is hard coded in the training phase, i.e. the loss of accuracy has to be caused by the weights which conduct transformation. This would be reduced by clipping weights.
- *TR to BVC*: The result of the transformation circuit is propagated to the BVC layer 1:1, i.e. there are no weights which can decrease accuracy. The head direction during training is chosen from only 20 possible directions. During simulation the head direction is more accurate, meaning that directions in-between two transformation layers will modulate transformation. While it has been shown by [5], [8], [9] and the simulations presented above, that those 20 layers are enough

5. Results and Discussion

to interpolate between maximally effective headings, the way the BVC profile is calculated is by addition of 2 or more layers, if the heading is between maximally effective headings. That means there will be some overlap resulting in the loss of accuracy.

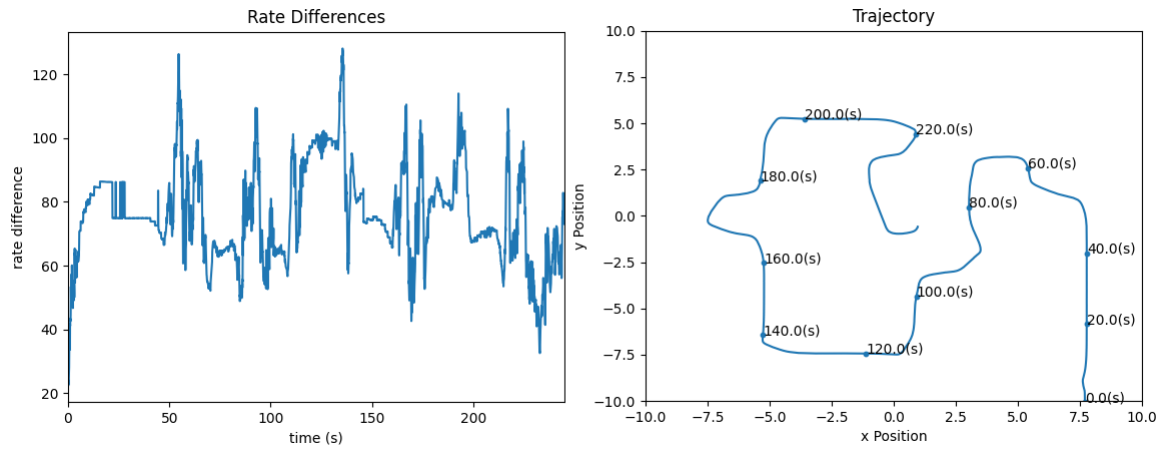


Figure 5.17.: (Left) Firing rate difference between eBC and BVC populations. (Right) trajectory of the robot with points indicating the location of the robot every 20 seconds. Robot moving through the regular maze environment (see figure 5.3). The maximum difference between firing rates was 125.70 and the mean was 79.63.

5. Results and Discussion

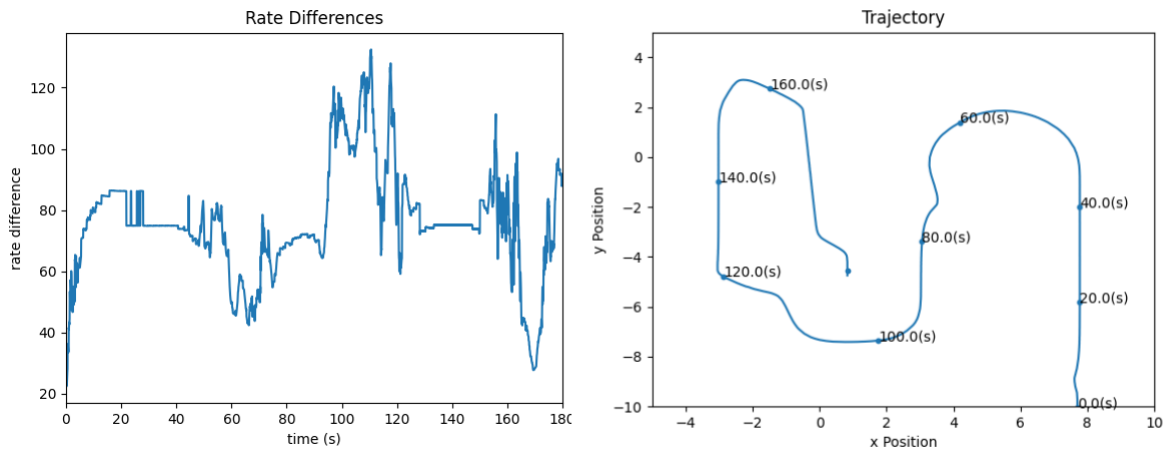


Figure 5.18.: (Left) Firing rate difference between eBC and BVC populations. (Right) trajectory of the robot with points indicating the location of the robot every 20seconds. Robot moving through the maze environment with curved turns (see figure 5.2). The maximum difference between firing rates was 125.43 and the mean was 78.53.

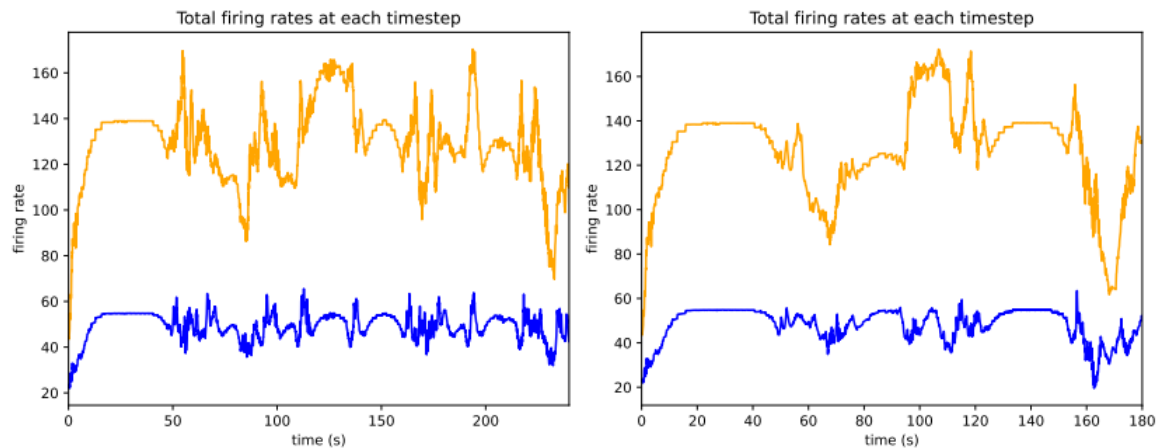


Figure 5.19.: Sum over firing rates of the eBC and BVC neuron populations at each time step. (Left) The robot was moving through the regular maze environment (see figure 5.3). (Right) The robot was moving through the maze environment with curved turns (see figure 5.2).

The remaining question is whether that is a flaw of the model or not. Intuitively it might even make sense that a mental transformation results in a loss of accuracy.

5. Results and Discussion

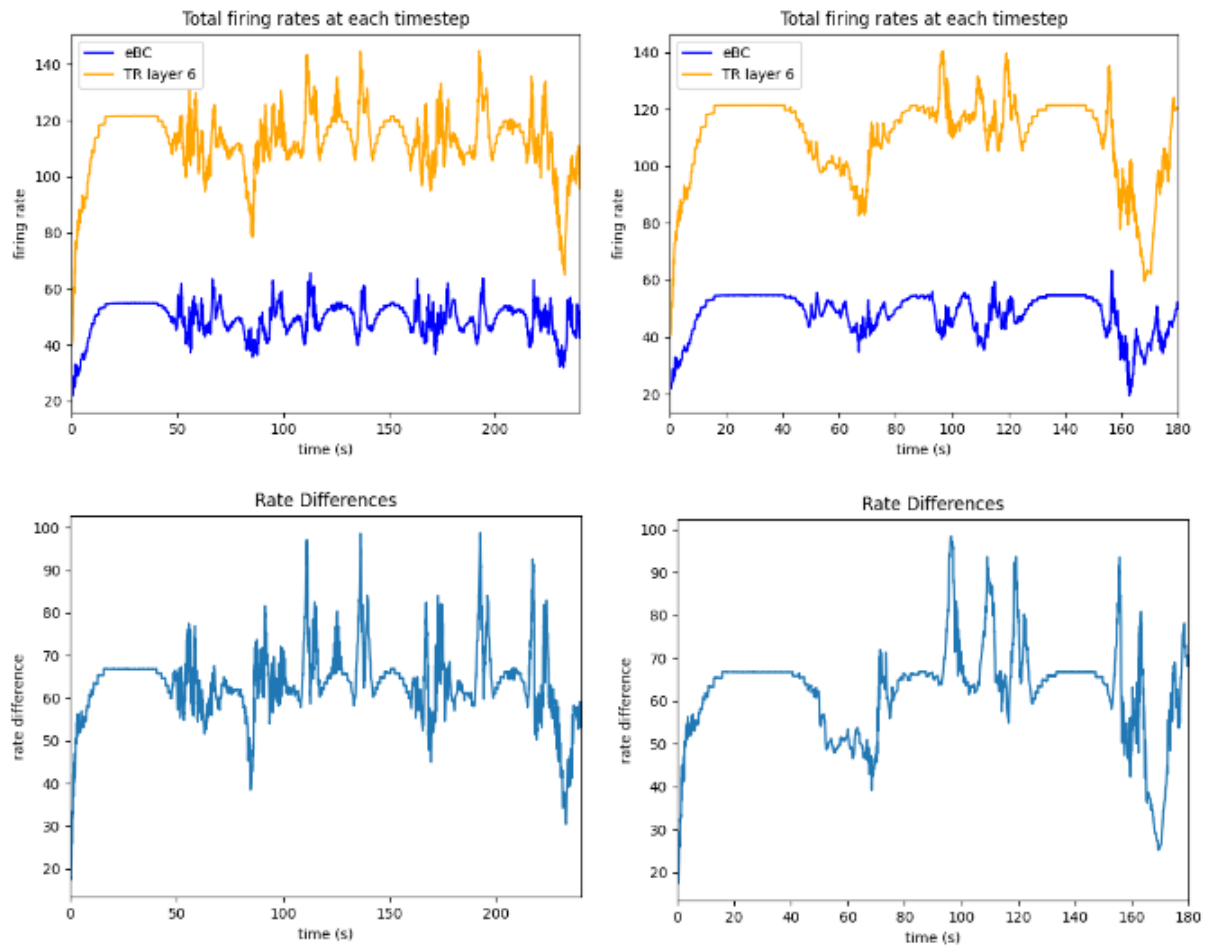


Figure 5.20.: (Left) Maze, (Right) Maze with curved turns. (Top) Sum over firing rates of the eBC and TR layer 6 neuron populations at each time step. (Bottom) Firing rate differences between eBC and TR layer 6 neuron populations.

That would imply that BVC receptive fields are bigger than receptive fields of eBCs. In training the same equation (equation 4.1) was used to calculate activity for eBC and BVC populations.

But during literature review no evidence was found, that the receptive fields are of the same size in brains. So this poses a question that has yet to be answered by neuroscientific research.

5.4. Biological Plausibility

The network, as discussed before consists of different parts which by themselves are all biologically plausible. The characteristics of BVC's [28], [18] and eBC's [16] used in this network are according to neuroscientific evidence. A boundary coding neuron has receptive fields tiling space around the agent, which increase in size with increasing distance, and fire depending on direction and distance of the boundary from the agent. There are only small differences to the neuroscientific data. The sensors used for the modelling are aligned all around the agent, thus the firing for boundaries in front and behind is the same. Although boundary coding cells have been reported to be firing for boundaries behind the animal it is not as accurate and strong as the firing in the animal's field of vision. It is most likely that firing behind the animal relies on mnemonic components [5]. Additionally BVC's are reported to fire in response to boundaries but drop-off edges and gaps as well [18], which is not simulated here. Since the allocentric BC firing is not coded in the reference frame of any sensory receptor there has to be circuitry that conducts reference frame transformation. To simulate that, the TR is incorporated. Recent studies [11], [23] provide strong experimental support for the predicted gain-field mechanism of egocentric–allocentric reference frame transformations for boundary coding, which is modulated by head direction signals [5]. Whether the seemingly bigger receptive fields, which result in wider firing fields in the BVC population are plausible or not, is as described, yet to be determined. The HDC network providing gain modulation, was modelled according to biological properties recorded from in-vivo head direction cells, by Amir El Sewisy.

6. Conclusion and Future Work

6.1. Conclusion

In this thesis I provided a model that encodes information about environmental surroundings and produces egocentric and allocentric boundary cell firing. Egocentric information encoded by egocentric boundary cells is transformed into an allocentric reference frame encoded by boundary vector cells. This transformation is conducted by a head direction modulated transformation circuit called the retrosplenial transformation circuit. The model worked adequately in the simulations shown in chapter 5, additionally it should work in any scenario as long as environmental information is fed into it in the right format (see chapter 4).

6.2. Future Work

Since the first discovery of Place Cells by O'Keefe and Dostrovsky in 1971[21] it has been shown that PCs are a very important aspect for spatial navigation. Place cells get input from different cells such as the Grid Cells. It was reported that PCs show adult like firing fields the first time they leave the nest at the age of 2.5 weeks, while GCs have variable and irregular fields until the fourth week. On the other hand BVCs express adult like firing fields as early as PCs [7]. Thus BVCs are very crucial for, and have been shown to drive PC firing. BVC activity drives place cells to fire [14], [12], [3], [4]. As future work this model should be incorporated into a model in which it will drive PCs to fire. This could then be used as a quantification measure as well. Comparing predicted place fields to in-vivo recordings from rat experiments.

The BB-model gives further theoretical foundation for such a model. It's modules and connections are based on neuroscientific, and psychological evidence, and are biologically plausible. But it is only tested in simulations, and for example the HDC network they used was not optimal. Thus using the architecture, but increasing the individual component's performances (such as the HDC network), and making them applicable to real-time scenarios would be worth to follow up on. Furthermore as mentioned before the mechanism providing input to the eBCs in this model would be one problem that has to be tackled in future work. The underlying mechanisms are yet

6. *Conclusion and Future Work*

to be fully understood and neuroscientific research has to provide results first. Yet, one example for a paper that tries to provide a model for distance and direction estimates to boundaries and objects (based on optic flow) is [24].

A. Computational Details

Simulations ran on an AMD Ryzen 5 3600 6-Core CPU, 16GB of RAM and a NVIDIA GeForce GTX 1060 6GB. The code for simulation was written in Python 3. In the simulation presented in Chapter 5, the robot is simulated in timesteps of 50ms. During the simulation, the neuron populations were visualized using matplotlib, see figure 5.5 for a sample visualization. The following computation times were recorded during simulation:

Regular Maze (figure 5.3):

- Total time (real): 124.65 s, Total time (simulated): 240.00 s
- Steps done BC-model simulation: 4800; Time: 53.19 s; 43.66% of total time
- Average step time HDC network: 0.45 ms
- Steps done HDC network: 24000; Time: 10.828 s; 8.81% of total time
- Average step time plotting: 65.49 ms
- Steps done plotting: 48; Time: 3.144 s; 2.56% of total time
- Average step time robot: 2.86 ms
- Steps done robot: 4800; Time: 13.71 s; 11.15% of total time

Maze with curved turns (figure 5.2):

- Total time (real): 93.37s, Total time (simulated): 180.00s
- Steps done BC-model simulation: 3600; Time: 40.71 s; 43.60% of total time
- Average step time HDC network: 0.45 ms
- Steps done HDC network: 18000; Time: 8.23 s; 8.63% of total time
- Average step time plotting: 65.55 ms
- Steps done plotting: 36; Time: 2.36 s; 2.48% of total time

A. Computational Details

- Average step time robot: 3.32 ms
- Steps done robot: 3600; Time: 11.96 s; 12.55% of total time

In both simulation environments the simulation time was approximately 1.93 times as fast as the simulated time. The times for different steps did not differentiate by a considerably between the simulation environments.

When plotting all 20 TR layers the simulation time increases drastically. Simulation time is approximately 0.17 times slower than simulated time. For a simulation run through the maze with curved turns it takes 1029s for a simulated time of 180s.

During training phase, in which weights were generated for the BC network following times were recorded:

- 1000 iterations: 19.80s
- 400.000 iterations: 7921.20 s / 132.02min / 2.2h

List of Figures

2.1.	Two receptive fields. The further away the boundary the bigger the receptive field [6].	4
2.2.	(Top) Firing rate map of a boundary vector cell. (Middle) Illustration of the receptive field of this cell, which is located at a fixed distance and direction from the agent. (Bottom) Vector pointing from the agent's location to the receptive field. When the receptive field is occupied by a boundary, the neuron fires. [6]	4
2.3.	Similar to 2.2 an illustration of a receptive field in allocentric coordinates. Dark red indicates the cell's tuning location. When a boundary is at the centre of the cell's receptive field the cell reaches it's peak firing rate. The cell's firing gradually increases with the boundary coming closer to the receptive field's centre.[18]	5
2.4.	When the animal is at a certain location a place cell fires. (Top) Firing rate depending on the animal's location, and the bottom image shows the receptive field. [6]	5
3.1.	Schematic of the BB-Model as described in section 3.1. Sensory inputs, rotation velocity and translational velocity are provided by the agent [5].	8
3.2.	Recording from a rat brain which shows how a grid cell is firing. (Left) The black trace shows the trajectory of a foraging rat in a square enclosure. Red dots are spike locations of the grid cell. Blue equilateral triangles have been drawn on top of the spike distribution to illustrate the regular hexagonal structure of the grid pattern. (Right) On the top is the same as on the left. The bottom is a color coded rate map with red showing high and blue showing low activity. [20]	9
4.1.	The single-neuron transfer function $\phi(x)$ defined in [22]	12
4.2.	Rate maps recorded in-vivo. On the top the black dots along the trajectory indicate spike locations of single neurons. Below the corresponding rate maps are illustrated [7].	14

List of Figures

4.3.	Activity profiles of eBC (left) and BVC (right) layers at the same time during simulation. All the neurons are arranged as described in section 4.3.1. Bright colors indicate a higher firing rate. Environmental surroundings are visualized by neuronal firing.	15
4.4.	Sixteen receptive fields along the 16 distance units. The closer to the agent the smaller the receptive field. The receptive fields shown here are all located on the same radian. The top left shows the receptive field closest to the agent and in the bottom right the receptive field furthest away from the agent is shown. Bright yellow indicates a higher firing rate (calculated according to Equation 4.1).	15
4.5.	Model schematic as described above in section 4.3.2	16
4.6.	Egocentric boundary information is shown in the eBC layer. The sublayers each encode the same egocentric map, but rotated. For simplicity only three sublayers are shown here. With heading direction at approx. 322° , sublayer 18, which is tuned to approximately 322° , is the layer which represents the current heading direction. The activity profile of sublayer 18 is then projected to the BVC layer while the others are inhibited[18].	18
4.7.	Neurons with receptive fields to the right and left in the egocentric reference frame are both connected to the same BVC in the allocentric reference frame.	18
5.1.	Pioneer P3DX equipped with 51 proximity sensors.	21
5.2.	Simulation environment: maze with round turns	22
5.3.	Simulation environment: maze	22
5.4.	Simulation environment: Maze with entry on the bottom left	22
5.5.	The agent is facing a decoded direction of 359.6° which is allocentric north. In the agent's peri-personal space there are walls left and right. The result is that the BVC and eBC activity profiles are approximately the same.	23
5.6.	The agent is facing a decoded direction of 90.7° which is allocentric west. In the agent's peri-personal space there are walls left and right, so the same as in figure 5.5. The transformation circuit rotates the representation by 90° and propagates that to the BVC layer, to produce allocentric representation in the BVC layer.	24

List of Figures

5.7. The agent is facing a decoded direction of 169.4° which is allocentric south. In the agent's peri-personal space there are walls left, right and behind. Due to the sensors being distributed all around the agent, the wall behind him is represented in the activity profile as well. This is only biologically plausible to some extent. It is expected that there is a mnemonic component involved that gives rise to BCs with a receptive field behind the agent. However this firing is like the agent has a 360° field-of-view. Discussed more in section 5.4.	24
5.8. The agent is facing a decoded direction of 100.6° which is allocentric west. In the agent's peri-personal space there are walls left, right, behind and in front of him producing a S like turn.	25
5.9. The agent is facing a decoded direction of 143.1° which is allocentric south-west. In the agent's peri-personal space there is a corner to the right, and a curved wall to the left. This scenario shows that the model is able to produce egocentric and allocentric firing that reflects curved surroundings.	25
5.10. The agent is facing a decoded direction of 43.1° which is allocentric north-west. In the agent's peri-personal space there is a corner to the right, and curved wall to the left. It is almost the same scenario as above in figure 5.9, but with a different heading.	26
5.11. The agent is facing a decoded direction of 110.41° which is approx. allocentric west. In the agent's peri-personal space there is a curved wall revolving around him from behind-right to front-right. To his left is a short wall. Different to scenarios 5.9 and 5.10 the wall is now to the right in a left turn. Both egocentric and allocentric produce accurate activity profiles.	26
5.12. The agent is facing a decoded direction of $262.8.0^\circ$ which is allocentric east. In the agent's peri-personal space he is surrounded by walls behind, left and in front of him, to his right there is the edge of a wall. Different from the other scenarios the agent is now moving east. The transformation circuit works just as good as while moving west and produces accurate BVC firing.	27
5.13. The agent is facing a decoded direction of 263.9° which is allocentric east. In his peri-personal space there are walls left, right and behind. Another scenario to show the transformation circuits functioning for heading east.	27

5.14. The agent is facing a decoded direction of 359.9° on the top and 0.1° on the bottom which is both allocentric north. In both Simulations the agent is in between two parallel walls. Normally the sensor length is 2.5. On the top the sensor length is halved to be 1.25 and on the bottom it is doubled to be 5. The result is, as described above in section 4.5, a change in how the environment is perceived in terms of space. On the top space seems wider, and on the bottom it seems narrower.	28
5.15. The agent is facing a decoded direction of 2.4° which is allocentric north. In his peri-personal space there are walls left and right. This is the same as in Figure 5.5, but with all 20 transformation layers plotted. It shows the counter-clockwise rotation of the eBC's activity profile through layers 1 to 20.	29
5.16. The agent is facing a decoded direction of 60.7° which is allocentric north-west. In his peri-personal space the surrounding environment is similar to Figure 5.11. Again all 20 transformation layers are plotted, and the figure shows the counter-clockwise rotation of the eBC's activity profile through layers 1 to 20. All the 20 layers represent the curvature of the wall to the right/allocentric north.	30
5.17. (Left)Firing rate difference between eBC and BVC populations. (Right) trajectory of the robot with points indicating the location of the robot every 20 seconds. Robot moving through the regular maze environment (see figure 5.3). The maximum difference between firing rates was 125.70 and the mean was 79.63.	32
5.18. (Left) Firing rate difference between eBC and BVC populations. (Right) trajectory of the robot with points indicating the location of the robot every 20seconds. Robot moving through the maze environment with curved turns (see figure 5.2). The maximum difference between firing rates was 125.43 and the mean was 78.53.	33
5.19. Sum over firing rates of the eBC and BVC neuron populations at each time step. (Left) The robot was moving through the regular maze environment (see figure 5.3). (Right) The robot was moving through the maze environment with curved turns (see figure 5.2).	33
5.20. (Left) Maze, (Right) Maze with curved turns. (Top) Sum over firing rates of the eBC and TR layer 6 neuron populations at each time step. (Bottom) Firing rate differences between eBC and TR layer 6 neuron populations.	34

List of Tables

4.1. Model parameters, re-used from [22] 12

Bibliography

- [1] [Online; accessed 9. Aug. 2021]. 2020. URL: https://www.in.tum.de/fileadmin/w00bws/i06/Thesis_Proposals/NeuralSLAM.pdf.
- [2] Andrew S. Alexander et al. "Egocentric boundary vector tuning of the retrosplenial cortex." In: *Sci. Adv.* 6.8 (2020), eaaz2322. ISSN: 2375-2548. DOI: 10.1126/sciadv.aaz2322.
- [3] Caswell Barry and Neil Burgess. "Learning in a geometric model of place cell firing." In: *Hippocampus* 17.9 (2007), pp. 786–800. ISSN: 1050-9631. DOI: 10.1002/hipo.20324.
- [4] Caswell Barry et al. "The boundary vector cell model of place cell firing and spatial memory." In: *Rev. Neurosci.* 17.1-2 (2006), p. 71. URL: <https://www.ncbi.nlm.nih.gov/pmc/articles/PMC2677716>.
- [5] Andrej Bicanski and Neil Burgess. "A neural-level model of spatial memory and imagery." In: *eLife* (2018). DOI: 10.7554/eLife.33752.
- [6] Andrej Bicanski and Neil Burgess. "Neuronal vector coding in spatial cognition." In: *Nat. Rev. Neurosci.* 21 (2020), pp. 453–470. ISSN: 1471-0048. DOI: 10.1038/s41583-020-0336-9.
- [7] Tale L. Bjercknes, Edvard I. Moser, and May-Britt Moser. "Representation of Geometric Borders in the Developing Rat." In: *Neuron* 82.1 (2014), pp. 71–78. ISSN: 0896-6273. DOI: 10.1016/j.neuron.2014.02.014.
- [8] Neil Burgess et al. "Memory for events and their spatial context: models and experiments." In: *Philos. Trans. R. Soc. London, Ser. B* 356.1413 (2001), pp. 1493–1503. ISSN: 1471-2970. DOI: 10.1098/rstb.2001.0948.
- [9] Patrick Byrne, Suzanna Becker, and Neil Burgess. "Remembering the past and imagining the future: a neural model of spatial memory and imagery." In: *Psychol. Rev.* 114.2 (2007), pp. 340–375. ISSN: 0033-295X. DOI: 10.1037/0033-295X.114.2.340. eprint: 17500630.
- [10] Erwin Coumans and Yunfei Bai. *PyBullet, a Python module for physics simulation for games, robotics and machine learning*. <http://pybullet.org>. 2016–2021.

- [11] Xenia Gofman et al. "Dissociation between Postrhinal Cortex and Downstream Parahippocampal Regions in the Representation of Egocentric Boundaries." In: *Curr. Biol.* 29.16 (2019), 2751–2757.e4. ISSN: 0960-9822. DOI: 10.1016/j.cub.2019.07.007.
- [12] Roddy Grieves, Eléonore Duvelle, and Paul Dudchenko. "A boundary vector cell model of place field repetition." In: *Spatial Cognition & Computation* 18.26 (2018), pp. 1–40. DOI: 10.1080/13875868.2018.1437621.
- [13] Torkel Hafting et al. "Microstructure of a spatial map in the entorhinal cortex - Nature." In: *Nature* 436 (2005), pp. 801–806. ISSN: 1476-4687. DOI: 10.1038/nature03721.
- [14] Tom Hartley et al. "Modeling Place Fields in Terms of the Cortical Inputs to the Hippocampus." In: *Hippocampus* 10.4 (2000), pp. 369–79. DOI: 10.1002/1098-1063(2000)10:4<369::AID-HIP03>3.0.CO;2-0.
- [15] D. O. Hebb. *The Organization of Behavior: A Neuropsychological Theory*. Andover, England, UK: Taylor & Francis, 2002. ISBN: 978-1-41061240-3. DOI: 10.4324/9781410612403.
- [16] James R. Hinman, G. William Chapman, and Michael E. Hasselmo. "Neuronal representation of environmental boundaries in egocentric coordinates." In: *Nat. Commun.* 10.2772 (2019), pp. 1–8. ISSN: 2041-1723. DOI: 10.1038/s41467-019-10722-y.
- [17] Øyvind Arne Høydal et al. "Object-vector coding in the medial entorhinal cortex - Nature." In: *Nature* 568 (2019), pp. 400–404. ISSN: 1476-4687. DOI: 10.1038/s41586-019-1077-7.
- [18] Colin Lever et al. "Boundary Vector Cells in the Subiculum of the Hippocampal Formation." In: *J. Neurosci.* 29.31 (2009), pp. 9771–9777. ISSN: 0270-6474. DOI: 10.1523/JNEUROSCI.1319-09.2009.
- [19] Tamas Madl et al. "Computational cognitive models of spatial memory in navigation space: A review." In: *Neural Networks* 65 (2015), pp. 18–43. ISSN: 0893-6080. DOI: 10.1016/j.neunet.2015.01.002.
- [20] May-Britt Moser, David Rowland, and Edvard Moser. "Place Cells, Grid Cells, and Memory." In: *Cold Spring Harbor perspectives in medicine* 5.1 (2015), a021808. DOI: 10.1101/cshperspect.a021808.
- [21] J. O'Keefe and J. Dostrovsky. "The hippocampus as a spatial map. Preliminary evidence from unit activity in the freely-moving rat." In: *Brain Res.* 34.1 (1971), pp. 171–175. ISSN: 0006-8993. DOI: 10.1016/0006-8993(71)90358-1.

- [22] Ulises Pereira and Nicolas Brunel. "Attractor Dynamics in Networks with Learning Rules Inferred from In Vivo Data." In: *Neuron* 99.1 (2018), 227–238.e4. ISSN: 0896-6273. DOI: 10.1016/j.neuron.2018.05.038.
- [23] Adrien Peyrache, Natalie Schieferstein, and Gyorgy Buzsáki. "Transformation of the head-direction signal into a spatial code - Nature Communications." In: *Nat. Commun.* 8.1752 (2017), pp. 1–9. ISSN: 2041-1723. DOI: 10.1038/s41467-017-01908-3.
- [24] Florian Raudies and Michael E. Hasselmo. "Modeling Boundary Vector Cell Firing Given Optic Flow as a Cue." In: *PLoS Comput. Biol.* 8.6 (2012), e1002553. ISSN: 1553-7358. DOI: 10.1371/journal.pcbi.1002553.
- [25] Emilio Salinas and Terrence J. Sejnowski. "Gain Modulation in the Central Nervous System: Where Behavior, Neurophysiology, and Computation Meet." In: *Neuroscientist : a review journal bringing neurobiology, neurology and psychiatry* 7.5 (2001), p. 430. DOI: 10.1177/107385840100700512.
- [26] Francesco Savelli, D. Yoganarasimha, and James J. Knierim. "Influence of boundary removal on the spatial representations of the medial entorhinal cortex." In: *Hippocampus* 18.12 (2008), pp. 1270–1282. ISSN: 1098-1063. DOI: 10.1002/hipo.20511. eprint: 19021262.
- [27] Trygve Solstad et al. "Representation of geometric borders in the entorhinal cortex." In: *Science* 322.5909 (2008), pp. 1865–1868. ISSN: 1095-9203. DOI: 10.1126/science.1166466. eprint: 19095945.
- [28] Sarah Stewart et al. "Boundary coding in the rat subiculum." In: *Philos. Trans. R. Soc. Lond. B Biol. Sci.* 369.1635 (2014). DOI: 10.1098/rstb.2012.0514.
- [29] J. S. Taube, R. U. Muller, and J. B. Ranck. "Head-direction cells recorded from the postsubiculum in freely moving rats. II. Effects of environmental manipulations." In: *J. Neurosci.* 10.2 (1990), pp. 436–447. ISSN: 0270-6474. DOI: 10.1523/JNEUROSCI.10-02-00436.1990.
- [30] Jeffrey Taube. "The Head Direction Signal: Origins and Sensory-Motor Integration." In: *Annu. Rev. Neurosci.* 30.1 (2007), pp. 181–207. DOI: 10.1146/annurev.neuro.29.051605.112854.